Nanoscale Res Lett (2010) 5:1518–1523
DOI 10.1007/s11671-010-9672-4

NANO EXPRESS

Aqueous Solution Preparation, Structure, and Magnetic Properties of Nano-Granular $Zn_xFe_{3-x}O_4$ Ferrite Films

Qiang Tian · Qian Wang · Qingshui Xie · Jiangong Li

Received: 11 March 2010 / Accepted: 7 June 2010 / Published online: 22 June 2010
© The Author(s) 2010. This article is published with open access at Springerlink.com

Abstract This paper reports a simple and novel process for preparing nano-granular $Zn_xFe_{3-x}O_4$ ferrite films ($0 \leq x \leq 0.99$) on Ag-coated glass substrates in DMAB-$Fe(NO_3)_3$-$Zn(NO_3)_2$ solutions. The deposition process may be applied in preparing other cations-doped spinel ferrite films. The Zn content x in the $Zn_xFe_{3-x}O_4$ films depends linearly on the Zn^{2+} ion concentration ranging from 0.0 to 1.0 mM in the aqueous solutions. With x increasing from 0 to 0.99, the lattice constant increases from 0.8399 to 0.8464 nm; and the microstructure of the films changes from the non-uniform nano-granules to the fine and uniform nano-granules of 50–60 nm in size. The saturation magnetization of the films first increases from 75 emu/g to the maximum 108 emu/g with x increasing from 0 to 0.33 and then decreases monotonously to 5 emu/g with x increasing from 0.33 to 0.99. Meanwhile, the coercive force decreases monotonously from 116 to 13 Oe.

Keywords Ferrite films · Aqueous solution deposition · Nano-granules · Magnetic properties

Introduction

Spinel ferrites, $Me_xFe_{3-x}O_4$ (Me = Mn, Co, Ni, Zn, Mg, Cu, etc.), are a technologically important group of materials, having numerous applications in magnetic devices, recording materials, photocatalysis, ferrofluid technology, magnetic refrigeration, and humidity sensors [1, 2]. The typical spinel ferrite, Fe_3O_4, has 64 tetrahedral sites (A sites) and 32 octahedral sites (B sites) of which only 8 A sites and 16 B sites are occupied by the Fe^{2+} and Fe^{3+} ions, respectively. The inverse nature of this spinel implies that all the A sites are occupied by Fe^{3+} ions, while an equal number of Fe^{2+} ions and Fe^{3+} ions share the B sites [3]. Structural and magnetic properties of spinel ferrites $MeFe_2O_4$ strongly depend upon the nature, concentration, and distribution of the substituted Me cations on A and B sites as well as the method of preparation. If the dependence of physical properties on substituted cations is known for a given complex ferrite, then it is possible to design a ferrite possessing the desired physical properties by choosing the appropriate compositions.

In recent years, the Zn- or NiZn- incorporated ferrite films with high resistivity and high permeability are widely used in micro-inductors, micro-transformers, magnetic recording, and high-frequency field [4]. For example, if the electronic circuits are covered with the NiZn ferrite film, the magnetic films render additional resistance to the circuits, thus attenuating the conducted-electromagnetic noises [5]. Fujiwara et al. studied the Zn^{2+} ions-doped ferrite films having high real part (μ') and imaginary part (μ'') of permeability in 10 to 100 MHz region. The films may be used as high-frequency magnetic film devices that are required at present for the current information technology infrastructure development [6]. $Zn_xFe_{3-x}O_4$ ferrite films were applied to field effect spintronic devices prepared by a pulsed-laser deposition technique [7].

Various preparation techniques such as liquid phase epitaxy, sputtering, plasma splay, and molecular beam epitaxy have been employed for preparing ferrite films. In all these processes, post-heat treatments or high deposition

Qiang Tian and Qian Wang contributed equally to this work.

Q. Tian · Q. Wang · Q. Xie · J. Li (✉)
Institute of Materials Science and Engineering and MOE Key Laboratory for Magnetism and Magnetic Materials, Lanzhou University, 730000 Lanzhou, China
e-mail: lijg@lzu.edu.cn

temperatures (>600°C) are required to induce the desired crystalline phases [8]. The high temperature would deteriorate the non-heat-resistant substrates, e.g., GaAs integrated circuits, plastics, and biomaterials [9]. The low-temperature wet chemical preparation methods such as spin spray plating [10], electrodeposition [11], and chemical deposition [12] offer a good alternative as it can overcome the drawbacks of the conventional methods. Abe et al. [13] developed a widely used spin spray method. In the process, long deposition time and complex equipment are needed; and a great deal of reactants is wasted. Recently, Izaki developed a very simple method to prepare magnetite and Zn-incorporated magnetite film by immersing a Pd/Ag-catalyzed substrate in the stable aqueous nitrate and dimethylamine borane complex (DMAB) solution [14, 15]. In Izaki's method, the incorporation of Zn into magnetite was finished by the deposition of magnetite film on ZnO thin film, so the Zn content of ferrite film and the magnetic properties cannot be well adjusted.

In order to overcome the drawbacks of the above-mentioned methods, a modified Izaki's method was used to prepare nanostructured $Zn_xFe_{3-x}O_4$ ferrite films ($0 \leq x \leq 0.99$) on Ag-coated glass substrates in the DMAB-$Fe(NO_3)_3$-$Zn(NO_3)_2$ solutions at 80°C by adjusting the $Zn(NO_3)_2$ concentration. The dependence of structure and magnetic properties of the $Zn_xFe_{3-x}O_4$ ferrite films on the Zn content was studied.

Experimental Section

Prior to deposition, glass substrates were cleaned ultrasonically in ethanol and acetone for removing organic impurities and rinsed in distilled water. Then Ag layer was deposited on the glass substrates (24 × 12 × 0.5 mm) using a two-step Sn/Ag activation process at room temperature. This two-step Sn/Ag activation process includes sensitizing the glass substrates by dipping in solution containing 10 g/l $SnCl_2$ and 0.08 M HCl, rinsing the substrates by distilled water, and activating the glass substrates by 1–2 g/l $AgNO_3$. The above steps were repeated three to six times to form Ag nano-granules with small sizes and a high density over the entire substrate surface. The $Zn_xFe_{3-x}O_4$ ferrite films ($0 \leq x \leq 0.99$) were prepared by immersing the Ag-catalyzed substrates in a 50-ml tube containing 15 mM iron nitrate 9-hydrate, 0–1.4 mM zinc nitrate hexahydrate, and 30 mM DMAB at 80°C for 1 h.

The pH values of the mixed solutions were measured by using a PHS-29A meter (Shanghai Precision Scientific Instrument Co.). X-ray diffraction (XRD) patterns of the films were measured using a Rigaku D/Max-2400 X-ray diffractometer with Cu K_α radiation (40 kV, 60 mA). The average grain sizes of the films were estimated from the diffraction peak widths through Scherrer equation. For the Rietveld refinements, the XRD data were recorded in a range from 15 to 90° (2θ) with a step width of 0.02° and a counting time of 3 s per step. The chemical compositions of the films were analyzed by a Thermo IRIS Advantage inductively coupled plasma atomic emission spectrometer (ICP-AES). The morphology and thickness of the films were analyzed by a Hitachi S-4800 field emission scanning electron microscope (SEM). The Raman spectra were recorded on the Horiba Jobin–Yvon LABRAM-HR800 laser micro-Raman spectrometer with 532-nm radiation that provides a typical spatial resolution less than 1 μm and spectral resolution better than 1 cm^{-1} in peak position. The magnetic properties of the films were measured at room temperature by a Lake Shore 7304 vibrating sample magnetometer (VSM).

Results and Discussion

No ferrite film could be deposited on the bare glass substrates under the same reaction conditions. So the Ag layer plays an important role in deposition of the ferrite films. The preparation of the Ag-catalyzed substrates can be formulated briefly as follows:

$$Sn^{2+} + 2Ag^{+} = Sn^{4+} + 2Ag \downarrow \quad (1)$$

The deposition of the ferrite film can be formulated briefly as follows: [8, 15, 16]

$$(CH_3)_2NHBH_3 + 3H_2O + H^{+} \rightarrow (CH_3)_2NH_2^{+} + H_3BO_3 + 3H_2 \uparrow, \quad (2)$$

$$(CH_3)_2NHBH_3 + 3H_2O \rightarrow (CH_3)_2NH_2^{+} + H_3BO_3 + 5H^{+} + 6e, \quad (3)$$

$$NO_3^{-} + H_2O + 2e \rightarrow NO_2^{-} + 2OH^{-}, \quad (4)$$

$$Fe^{3+} + e \rightarrow Fe^{2+}, \quad (5)$$

$$xFe^{2+} + yFe^{3+} + zZn^{2+} + 8OH^{-} \rightarrow (Fe^{2+}, Fe^{3+}, Zn^{2+})_3(OH)_8 \ (x + y + z = 3), \quad (6)$$

$$(Fe^{2+}, Fe^{3+}, Zn^{2+})_3(OH)_8 \rightarrow (Fe^{2+}, Fe^{3+}, Zn^{2+})_3O_4 + 4H_2O. \quad (7)$$

The pH value increases from 2.2 to 4.2 in the first 20 min and subsequently decreases slightly in the range from 4.2 to 3.9. At the beginning of the reaction, the low pH value (pH = 2.2) is caused by the hydrolyzation of Fe^{3+}. The H^{+} ions are rapidly reduced to H_2, and DMAB is oxidized to weak basic dimethylamine according to Eq. 2. The NO_3^{-} ions are also reduced to NO_2^{-} ions, giving rise to an increase in the OH^{-} concentration and an increase in the pH value of the solution to 4.2 (Eq. 4). With the progress of the reaction, the OH^{-} ions and metal cations are consumed

gradually (Eq. 6), which leads to a slight decrease in pH value from 4.2 to 3.9. However, the magnetite grows only at pH > 7 according to the potential-pH equilibrium diagram for the iron-water system at 25°C [17]. Homma et al. [18] found that the oxidation of DMAB preferably proceeded in the electric double layer at the surface region of the catalyzed metal; and the catalytic activity of the deposited metal was caused by its electron acceptivity. The hydrolyzed metal ions migrate to the surface of the Ag layer mediated by the electrostatic force, and the dehydration reaction is accompanied by the reactions of Eqs. 6 and 7. The reduction of NO_3^- ions to NO_2^- ions is accelerated at the surface of the Ag layer, which is the key to raising the local pH value. Therefore, the ferrite films can form at a weak acid solution. In addition, as shown in Fig. 1, the Ag-catalyzed layer on the glass substrates is composed of fine Ag nano-granules of 1–10 nm in size. The surface of the Ag layer possesses the large surface area of the fine Ag nano-granules. Heterogeneous nucleation is promoted by the presence of the Ag nano-granules on the glass substrates and energetically more favorable due to the high surface energy of the large surface area of the fine Ag nano-granules. The nucleation may take place at a lower saturation ratio on the Ag-catalyzed substrates than in solution.

The compositions of the prepared $Zn_xFe_{3-x}O_4$ films were determined by ICP-AES measurement. The Zn contents x in the $Zn_xFe_{3-x}O_4$ films prepared with the $Zn(NO_3)_2$ concentrations of 0, 0.1, 0.25, 0.4, 0.6, 0.8, 1.0, and 1.2 mM in solution are 0, 0.12, 0.33, 0.41, 0.64, 0.77, 0.96, and 0.99, respectively. Meanwhile, the Fe content in the films decreases from 3 to 2.01 as x increases from 0 to 0.99. The Zn content x in the $Zn_xFe_{3-x}O_4$ films depends linearly on the Zn^{2+} ion concentration ranging from 0.0 to 1.0 mM in the solutions, as shown in Fig. 2. This is helpful for preparing Zn ferrite films with desired Zn contents. The impurities (mainly B) in the $Zn_xFe_{3-x}O_4$ ferrite films are less than 0.05 wt%.

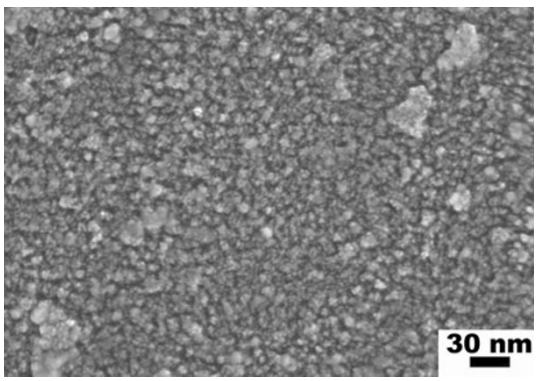

Fig. 1 The SEM micrograph of the Ag-catalyzed substrate surface

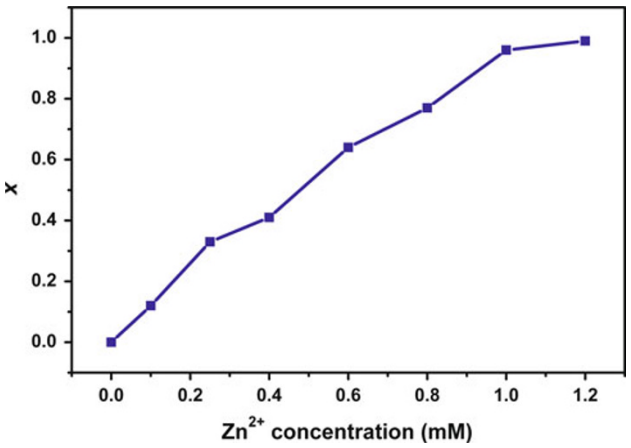

Fig. 2 The dependence of the zinc content x in the films on the zinc ion concentration in the solutions

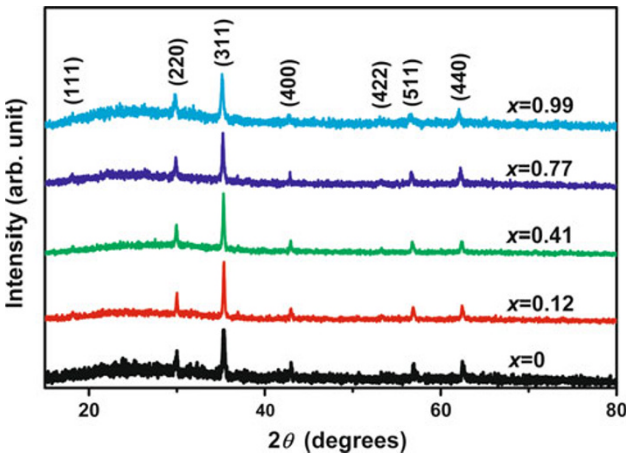

Fig. 3 The XRD patterns of the $Zn_xFe_{3-x}O_4$ ferrite films with $x = 0$, 0.12, 0.41, 0.77, and 0.99

Figure 3 shows the XRD patterns of the $Zn_xFe_{3-x}O_4$ ferrite films with the x values of 0, 0.12, 0.41, 0.77, and 0.99. All the observed diffraction peaks can be indexed as the (111), (220), (311), (400), (422), (511), and (440) diffractions of the cubic spinel phase [3, 19]; and no additional diffraction peaks of any other phases are detected. The diffraction peaks in the XRD patterns of all the films are broader compared to the coarse-grained spinel, indicating that the grains of the ferrite films are fine. The average grain sizes of the $Zn_xFe_{3-x}O_4$ films with the x values of 0, 0.12, 0.41, 0.77, and 0.99 estimated using Scherrer formula from the widths of the diffraction peaks are 47, 44, 49, 45, and 32 nm, respectively. All diffraction peaks in the XRD patterns shift slightly toward low angles with increasing Zn content, indicating that the lattice constant of the $Zn_xFe_{3-x}O_4$ films increases with increasing Zn content. The lattice constants for the films with different Zn contents determined by the Rietveld refinements are shown in Fig. 4. The lattice constant increases from 0.8399

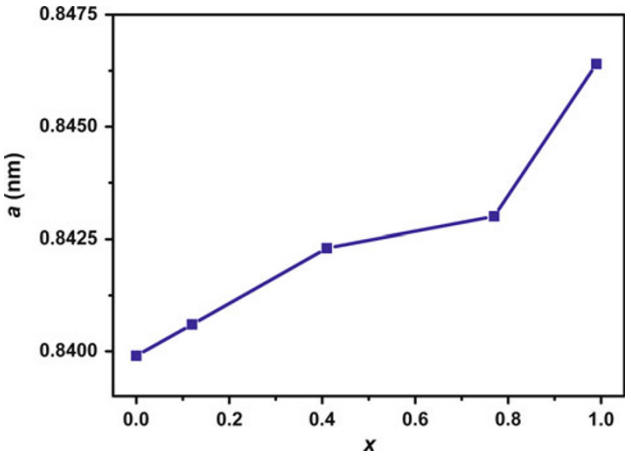

Fig. 4 The lattice constant a of the $Zn_xFe_{3-x}O_4$ ferrite films in variation of the Zn content x

to 0.8464 nm as x increases from 0 to 0.99. This result is similar to the Zn ferrites and NiZn ferrites prepared by pulsed-laser deposition and sol–gel method [7, 20]. It may be understood by considering that the ionic radius of Zn^{2+} (0.074 nm) is larger than the ionic radius of Fe^{3+} (0.064 nm) [21, 22]. The incorporation of larger ions into the lattice of the films would expand the lattice and increase the lattice constant.

The Fe_3O_4 film was composed of nano-granules 10–250 nm in size (Fig. 5a). The $Zn_{0.41}Fe_{2.59}O_4$ and $Zn_{0.99}Fe_{2.01}O_4$ ferrite films are composed of uniform equiaxed nano-granules of about 50–60 nm in size (Fig. 5b, c). This indicates that the incorporation of Zn^{2+} ions into the ferrite films leads to the formation of fine and uniform nano-granules. The $Zn_{0.41}Fe_{2.59}O_4$ ferrite film has a slightly rough surface with a thickness of about 300 nm (Fig. 5d). The nano-granular microstructure of the deposited ferrite films may result from the random nucleation of the ferrite granules on the nano-granular surface of the Ag catalyzed layer on the glass substrates (Fig. 1). However, for the spin spray method, the smooth bare glass was directly used as the reaction substrates that can facilitate the nucleation and growth of ferrite grains to columnar microstructure [6].

The magnetite (Fe_3O_4) has a cubic structure belonging to the space group O_h^7 ($Fd3\ m$). Theoretical analysis for the spinel ferrite showed that there are five Raman-active modes ($A_{1g} + E_g + 3T_{2g}$) that involve mainly the motion of the O ions and both the O and the ions in A sites and do not contain the vibration of the ions in B sites at all [23, 24]. Figure 5 shows the Raman spectra measured at 293 K for the Fe_3O_4, $Zn_{0.41}Fe_{2.59}O_4$, and $Zn_{0.77}Fe_{2.23}O_4$ films. There are three obvious Raman-active modes at about 302, 535, and 671 cm^{-1} for the Fe_3O_4 film, and other two Raman-active modes are absent. This result is in agreement with the reported studies [25]. In the cubic spinels including ferrites, the modes at above 600 cm^{-1} are of the A_{1g} type, mostly corresponding to the motion of oxygen in tetrahedral AO_4 groups. With increasing Zn content, the Raman mode around 680 cm^{-1} becomes broad and shifts slightly toward high frequency as shown in Fig. 6. The Raman mode at 680 cm^{-1} for the $Zn_{0.77}Fe_{2.23}O_4$ film was fitted by two Gauss peaks with the peak positions at 653 and 681 cm^{-1}. The mode for the $Zn_{0.41}Fe_{2.59}O_4$ film was fitted by two peaks at 648 and 679 cm^{-1}. In fact, the Raman modes at 653 and 648 cm^{-1} are ascribed to the oxygen breathing vibrations against zinc; and the 681 and

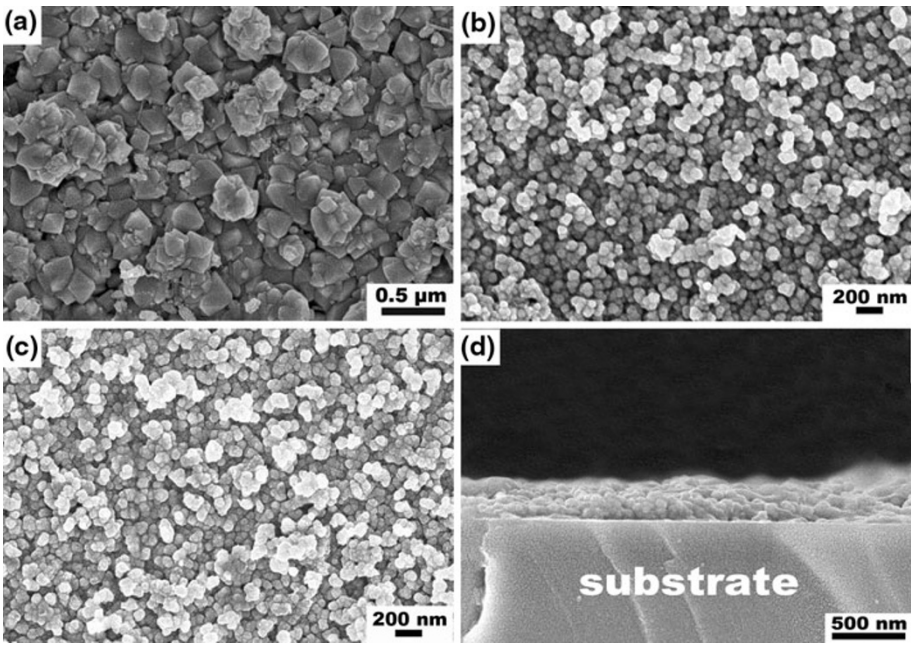

Fig. 5 The top view SEM micrographs of the Fe_3O_4 (**a**), $Zn_{0.41}Fe_{2.59}O_4$ (**b**), and $Zn_{0.99}Fe_{2.01}O_4$ (**c**) ferrite films as well as the cross-sectional SEM image of the $Zn_{0.41}Fe_{2.59}O_4$ ferrite film (**d**)

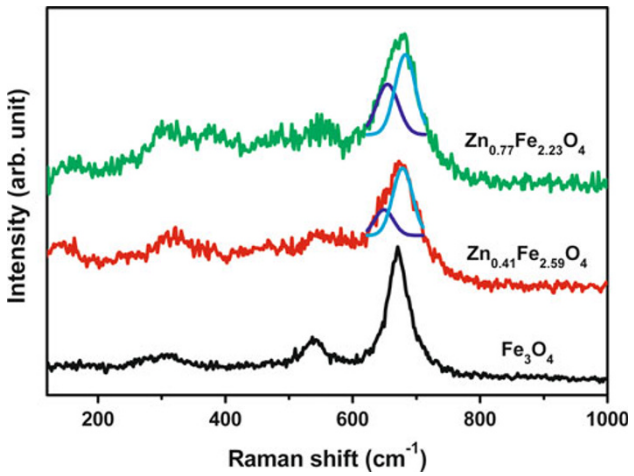

Fig. 6 The Raman spectra for the Fe_3O_4, $Zn_{0.41}Fe_{2.59}O_4$, and $Zn_{0.77}Fe_{2.23}O_4$ films

679 cm^{-1} modes are due to corresponding oxygen vibrations against iron [23]. So the observation of the broad mode at around 680 cm^{-1} can be the result of the coexistence of FeO_4 and ZnO_4 groups [4]. In addition, the intensity ratio of the ZnO_4 vibration to the FeO_4 vibration increases with increasing Zn content. Hence, more Zn^{2+} ions are incorporated into the A sites with increasing x for $Zn_xFe_{3-x}O_4$.

The saturation magnetization M_s increases with x increasing from 0 to 0.33, reaches a maximum value of 108 emu/g at $x = 0.33$, and then decreases to 5 emu/g with x further increasing from 0.33 to 0.99 as shown in Fig. 7. The M_s of the $Zn_xFe_{3-x}O_4$ film samples prepared by spin spray method increases with increasing x, reaches a maximum value of 110 emu/g at $x \approx 0.25$, and then decreases with further increase in x [6]. The variation of the M_s of the $Zn_xFe_{3-x}O_4$ ferrite films can be attributed to the ion distribution and the change in interactions between the A and

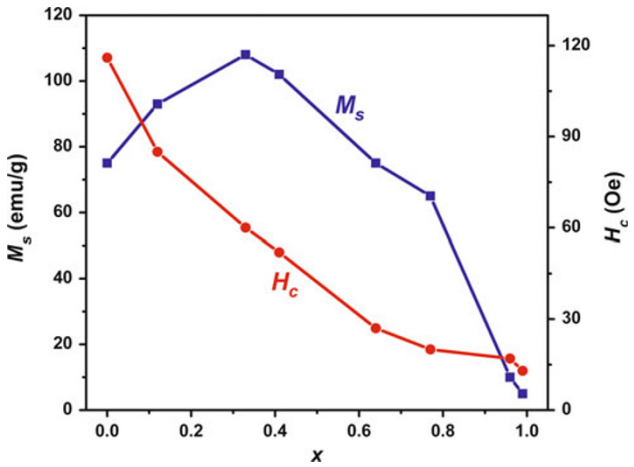

Fig. 7 The saturation magnetization M_s and coercivity H_c for the $Zn_xFe_{3-x}O_4$ ferrite films in variation of the Zn content x

B sites. From the Raman spectra analysis result and the reported results [26, 27], the Zn^{2+} ions occupy the A sites, while the Fe^{3+} ions are distributed over both A and B sites in the spinel structure. Hence, the magnetization per spinel unit cell of $Zn_xFe_{3-x}O_4$ can be described as

$$\left[Zn_x^{II}Fe_{1-x}^{III}\right]_A\left[Fe_{1-x}^{II}Fe_{1+x}^{III}\right]_B O_4. \quad (8)$$

At low Zn concentrations, the magnetic moments of the A sites are antiparallel to those of the B sites, so the net magnetic moment of the $Zn_xFe_{3-x}O_4$ spinel unite cell is the difference in the magnetic moment between B and A sites [28, 29]. Therefore, the net magnetic moment m of the $Zn_xFe_{3-x}O_4$ spinel unite cell is

$$m = m_B - m_A = (4 + 6x)\mu_B. \quad (9)$$

For $x < 0.33$, as x increases, the m increases; so the M_s of the $Zn_xFe_{3-x}O_4$ ferrite films increases with increasing x. However, at high Zn contents, the total magnetization is expressed by

$$m = m_B \cos \alpha_{YK} - m_A, \quad (10)$$

where α_{YK} is the canting angle (Yafet-Kittel angle) between the moments in the B sites [30]. For $x > 0.33$, the magnetic moments of the remaining Fe^{3+} ions in the A sites are no longer able to align all the moments of the iron ions in the B sites antiparallel to the moments of Fe^{3+} ions in the A sites. The B sites will then divide themselves into sublattices, and the magnetic moments of which have a canting angle with each other [30, 31]. So the further replacement of the Fe^{3+} ions by the Zn^{2+} ions leads to a decrease of the magnetic moments in the B sites and hence decreases the total magnetization.

Figure 7 shows that the coercive force H_c decreases monotonously from 116 to 13 Oe with x increasing from 0 to 0.99. The variation of the H_c can be explained by the inverse relation between H_c and M_s, $H_c \propto K_1/M_s$, where K_1 is the anisotropy constant [32], which decreases with increasing Zn content [26]. Decrease in K_1 and increase in M_s with x increasing from 0 to 0.33 lead to a decrease of H_c. For $x > 0.33$, both K_1 and M_s decrease with increasing x. It implies that the decrease of K_1 ($K_1 = -1.1 \times 10^4$ J/m^3 for Fe_3O_4 and $K_1 = 0$ for $ZnFe_2O_4$) is the dominant factor compared to the decrease of M_s. Although H_c decreases with increasing Zn content, the H_c values are a little larger than those of the $Zn_xFe_{3-x}O_4$ films with the same compositions prepared by the spin spray method [6]. The H_c of the $Zn_xFe_{3-x}O_4$ films prepared by the spin spray method decreases from 100 to 5 Oe with x increasing from 0 to 0.7 [6]. First, it may be due to the small grain size in the films that can induce large K_1 [33]. Second, it may be attributed to the rough surface, which provides pinning sites for domain walls [34].

Conclusions

The $Zn_xFe_{3-x}O_4$ ($0 \leq x \leq 0.99$) ferrite films were deposited in the DMAB-$Fe(NO_3)_3$-$Zn(NO_3)_2$ solutions at low temperature (80°C) on the Ag-coated glass substrates. The Zn content x in the $Zn_xFe_{3-x}O_4$ films increases linearly with the Zn^{2+} ion concentration in the solution. As x increases from 0 to 0.99, the lattice constant of the films increases from 0.8399 to 0.8464 nm; and the microstructure of the films change from the non-uniform nano-granules to the fine and uniform nano-granules of 50–60 nm in size. The saturation magnetization of the $Zn_xFe_{3-x}O_4$ films first increases from 75 emu/g to the maximum 108 emu/g with x increasing from 0 to 0.33 and then decreases to 5 emu/g with x increasing from 0.33 to 0.99. Meanwhile, the coercive force decreases monotonously from 116 to 13 Oe with x increasing from 0 to 0.99.

Acknowledgments The work was supported by the National Natural Science Foundation of China under grant No. 50872046, the International S&T Cooperation Program (ISCP) under grant No. 2008DFA50340, MOST, and the Specialized Research Foundation for the Doctoral Programs under grant No. 20070730022, MOE, China.

Open Access This article is distributed under the terms of the Creative Commons Attribution Noncommercial License which permits any noncommercial use, distribution, and reproduction in any medium, provided the original author(s) and source are credited.

References

1. H.L. Zhu, D.R. Yang, L.M. Zhu, Surf. Coat. Technol. **201**, 5870 (2007)
2. S.-H. Yu, M. Yoshimura, Adv. Funct. Mater. **12**, 9 (2002)
3. L.K.C. de Souza, J.R. Zamian, G.N. da Rocha Filho, L.E.B. Soledade, I.M.G. dos Santos, A.G. Souza, T. Scheller, R.S. Angéica, C.E.F. da Costa, Dyes Pigments **81**, 187 (2009)
4. Q. Tian, J. Li, Q. Wang, S. Wang, X. Zhang, Thin Solid Films **518**, 313 (2009)
5. K. Kondo, T. Chiba, H. Ono, S. Yoshida, Y. Shimada, N. Matsushita, M. Abe, J. Appl. Phys. **93**, 7130 (2003)
6. A. Fujiwara, M. Tada, T. Nakagawa, M. Abe, J. Magn. Magn. Mater. **320**, 67 (2008)
7. J. Takaobushi, H. Tanaka, T. Kawai, S. Ueda, J. Kim, M. Kobata, M. Yabashi, K. Kobayashi, Y. Nishino, D. Miwa, K. Tamasaku, T. Ishikawa, Appl. Phys. Lett. **89**, 242507 (2006)
8. M. Abe, Electrochim. Acta **45**, 3337 (2000)
9. M. Abe, T. Ishihara, Y. Kitamoto, J. Appl. Phys. **85**, 5705 (1999)
10. J. Miyasaka, M. Tada, M. Abe, N. Matsushita, J. Appl. Phys. **99**, 08M916 (2006)
11. S.D. Sartale, G.D. Bagde, C.D. Lokhande, M. Giersig, Appl. Surf. Sci. **182**, 366 (2001)
12. Y. Saito, K. Kaga, M. Tsutsumida, H. Unuma, Chem. Lett. **34**, 1202 (2005)
13. M. Abe, Y. Tamauta, Y. Goto, N. Kitamura, M. Gomi, J. Appl. Phys. **61**, 3211 (1987)
14. M. Izaki, O. Shinoura, Adv. Mater. **13**, 142 (2001)
15. M. Izaki, A. Takino, N. Fujita, T. Shinagawa, M. Chigane, S. Ikeda, M. Yamaguchi, K. Arai, A. Tasaka, J. Electrochem. Soc. **151**, C519 (2004)
16. M. Chigane, M. Izaki, Y. Hatanaka, T. Shinagawa, M. Ishikawa, Thin Solid Films **515**, 2513 (2006)
17. M. Pourbaix, *Altas of Electrochemical Equilibria in Aqueous Solution* (Pergamon Press, London, 1966)
18. T. Hommaa, A. Tamaki, H. Nakai, T. Osaka, J. Electroanal. Chem. **559**, 131 (2003)
19. E. Veena Gopalan, I.A. Al-Omari, K.A. Malini, P.A. Joy, D.S. Kumar, Y. Yoshida, M.R. Anantharaman, J. Magn. Magn. Mater. **321**, 1092 (2009)
20. L. Wang, F.S. Li, J. Magn. Magn. Mater. **223**, 233 (2001)
21. H.-I. Hsiang, Y.-L. Liu, J. Alloys Compd. **472**, 516 (2009)
22. M. Ajmal, A. Maqsood, J. Alloys Compd. **460**, 54 (2008)
23. M. Maletin, E.G. Moshopoulou, A.G. Kontos, E. Devlin, A. Delimitis, V.T. Zaspalis, L. Nalbandian, V.V. Srdic, J. Eur. Ceram. Soc. **27**, 4391 (2007)
24. D.M. Phase, S. Tiwari, R. Prakash, A. Dubey, V.G. Sathe, R.J. Choudhary, J. Appl. Phys. **100**, 123703 (2006)
25. O.N. Shebanova, P. Lazor, J. Solid State Chem. **174**, 424 (2003)
26. A. Verma, T.C. Goel, R.G. Mendiratta, P. Kishan, J. Magn. Magn. Mater. **208**, 13 (2000)
27. C. Upadhyay, H.C. Verma, S. Anand, J. Appl. Phys. **95**, 5746 (2004)
28. H. Kavas, A. Baykal, M.S. Toprak, Y. Köseoğlu, B. Aktas, M. Sertkol, J. Alloys Compd. **479**, 49 (2009)
29. S. Liang, R.J. Gambino, S. Sampath, M.M. Raja, J. Appl. Phys. **99**, 08M915 (2006)
30. J. Smit, H.P.J. Wijn, *Ferrites* (Philips Technical Library, Eindhoven, 1959)
31. Y. Li, Q. Li, M. Wen, Y. Zhang, Y. Zhai, Z. Xie, F. Xu, S. Wei, J. Electron Spectrosc. Relat. Phenom. **160**, 1 (2007)
32. J.M.D. Coey, *Rare-Earth Permanent Magnetism* (Wiley, New York, 1996)
33. M. Pal, P. Brahma, D. Chakravorty, D. Bhattacharyya, H.S. Maiti, J. Magn. Magn. Mater. **164**, 256 (1996)
34. M. Taheri, E.E. Carpenter, V. Cestone, M.M. Miller, M.P. Raphael, M.E. McHenry, V.G. Harris, J. Appl. Phys. **91**, 7595 (2002)